

Article

Micropaleontological and Isotopic Perspective of Surface Water Mass Variability in the NE Atlantic from MIS 6 to 5e (188 to 115 ka)

Harunur Rashid ^{1,2,*}, Jiaxin Chen ¹, Mary Menke ² and Min Zeng ¹¹ College of Marine Sciences, Shanghai Ocean University, Shanghai 201306, China² School of Earth Sciences, Ohio State University, Columbus, OH 43210, USA

* Correspondence: harunurbhola@gmail.com

Abstract: The penultimate glaciation (marine isotope stage (MIS) 6) is considered regionally extreme compared to the last glacial maximum, in which the European ice sheets had a vast areal extent. In contrast to the last deglaciation (19–7 ka), the penultimate deglaciation (140–130 ka) hosts one of the most rapid oceanographic changes of the late Pleistocene. In this study, we reconstructed changes in the near-surface and thermocline in the central to northeast Atlantic by analyzing sediments from two Integrated Ocean Drilling Program Expedition 306 sites. Sites U1313 (41°00.6' N, 32°57.4' W) and U1314 (56°21.9' N, 27°53.3' W) were drilled on the eastern flank of the mid-Atlantic ridge and Gardar Drift of the eastern subpolar North Atlantic, respectively. We analyzed planktonic foraminiferal assemblages, ice-rafted debris (IRD), and oxygen isotopes in two planktonic foraminifers, *Globigerina bulloides*, and *Globorotalia inflata*, from MIS 6 to 5e (185–115 ka). Warmer and colder sea-surface conditions were marked by a change in the relative abundance of polar, subpolar, and transitional planktonic foraminifers. Oxygen isotopes in *G. bulloides* and *G. inflata* suggest that the thermocline deepened at the subtropical Site U1313 during MIS 6. The lack of *Globorotalia inflata* prevented us from profiling the mixed layer and thermocline at the subpolar Site U1314. In contrast to MIS 6, the mixed layer and thermocline were re-stratified during the last interglacial. The lack of major IRD events at both sites suggests the stability of the Laurentide ice sheet during MIS 6 compared to the subsequent glaciation. The presence of Heinrich event 11 indicates the discharge of freshwater that freshened the sea surface, resulting in mixing between the mixed layer and thermocline. Our results were placed into a broader context using published data that shed light on the sensitivity of freshwater discharge to the North Atlantic and the following changes with a transition from a penultimate glacial to an interglacial period in surface circulation.

Keywords: MIS 6 and 5e; subpolar and subtropical gyre; foraminiferal assemblages; oxygen isotopes; ice-rafted debris



Citation: Rashid, H.; Chen, J.; Menke, M.; Zeng, M. Micropaleontological and Isotopic Perspective of Surface Water Mass Variability in the NE Atlantic from MIS 6 to 5e (188 to 115 ka). *Geosciences* **2023**, *13*, 149. <https://doi.org/10.3390/geosciences13050149>

Academic Editors: Angelos G. Maravelis and Jesus Martinez-Frias

Received: 25 January 2023

Revised: 28 April 2023

Accepted: 9 May 2023

Published: 15 May 2023



Copyright: © 2023 by the authors. Licensee MDPI, Basel, Switzerland. This article is an open access article distributed under the terms and conditions of the Creative Commons Attribution (CC BY) license (<https://creativecommons.org/licenses/by/4.0/>).

1. Introduction

Past studies suggest that the European ice sheets attained their largest extent during the penultimate glaciation (MIS 6) compared to the last glacial maximum of the last glacial cycle [1,2]. Consequently, the numerous ice-rafted debris (IRD) events identified on the European continental margin of the North Atlantic were attributed to the instability of the European ice sheets during MIS 6. Using sediments from the Ocean Drilling Program (ODP) Site 980 at Feni Drift, McManus et al. [3] documented minor IRD peaks, sea-surface cooling, and freshening, yet these IRD events are subdued compared to the IRD events (i.e., Heinrich events) of the last glacial cycle. Further, Mokeddem and McManus [4] also reported five IRD peaks from the eastern subpolar gyre at ODP Site 984 on the Bjorn Drift during MIS 6. The authors suggested that these IRD events were equivalent to the Dansgaard–Oeschger interstadial events of the last glacial cycle [5,6]. However, the lack of detrital carbonate grains suggests that those IRD events originated from the European ice sheets. Using

a suite of paleo proxies, including the concurrent planktonic and benthic foraminiferal oxygen isotopes, Morkkedem and McManus [4] suggested diminished stratification between the surface and deep waters in the Iceland Basin. Kandiano and Bauch [7] have reported various sea-surface characteristics from core M23414 within the transitional water of the North Atlantic. However, the millennial-scale events recorded at Site 984 and their impact on the sea-surface characteristics are incompletely understood due to the coarse temporal resolution. In the subtropical region of the central North Atlantic at Deep Sea Drilling Project (DSDP) Site 607, the southern edge of the so-called IRD belt, Ruddiman et al. [8] reported foraminiferal assemblage data without IRD and oxygen isotopes in planktonic foraminifers. Chapman et al. [9] reported foraminiferal assemblage and IRD data from core SU90-03, ~122 km south of Site 607, for the past 150 ka. Using sediments from Integrated Ocean Drilling Program (IODP) Site U1313, which was the reoccupation of DSDP Site 607, Naafs et al. [10] reported changes in the sea-surface temperature using alkenones but did not report IRD. Further, Smith et al. [11] also reported coarse resolution sea-surface characteristics (i.e., IRD/g and counting of five dominant planktonic foraminifers) from Site U1313 during MIS 6, but due to the lack of complete profiling of the upper water column (i.e., mixed layer and thermocline), the impact of freshwater on the sea surface is poorly known.

Detailed studies about the last deglaciation and Termination 1 (T1, 14.50 ka; [12]) surrounding the North Atlantic provides the nature and extent of abrupt climate changes (e.g., the Younger Dryas, Bolling–Allerod, etc.) and reorganization of circulation [5,13–16]. However, such detailed studies about the penultimate deglaciation, including Termination 2 (T2; 129.04 ± 0.07 ky; [12]) compared to T1, are scarce, although a few studies and reviews shed some light on variability in the sea-surface characteristics [9,17–23] and deep ocean reorganization [21,24,25]. Notably, the transition from the penultimate glacial to interglacial between 140 and 130 ka is considered one of the most rapid oceanographic changes of the Quaternary period [23,26,27]. Due to the rise in solar insolation, ice sheets surrounding the North Atlantic disintegrated, resulting in an ~80 m rise in sea level in which the H11 iceberg rafting event nested within the penultimate deglaciation [28–31]. As a result, cold and dry conditions, reminiscent of the climate during the last glaciation surrounding the North Atlantic, prevailed [20,21,32]. It is suggested that the H11 freshwater input perturbed the mixed layer and thermocline, which might have forced many planktonic foraminifers to deeper waters [28,32]. These changes must have affected the subpolar, North Atlantic transitional, and subtropical waters. However, the extent to which the degree of changes occurred between the subpolar and subtropical latitudes is poorly understood due to the lack of data.

In the present study, we reconstruct the sea-surface, near-surface, and thermocline conditions during the penultimate glaciation (MIS 6) to deglaciation (MIS 6–5e) and the warmest part of the last interglacial (i.e., MIS 5e). We have employed foraminiferal assemblage and IRD counts with oxygen isotopes in two mixed layer and thermocline planktonic foraminifers, *Globigerina bulloides* and *Globorotalia inflata*, from sediment samples of two IODP sites U1313 [11] and U1314 in the North Atlantic. Our data suggest that the subtropical Site U1313 recorded incursion of the subpolar and transitional waters while the subpolar Site U1314 witnessed polar and Arctic waters during MIS 6. Our data further suggest that the mixed-and-thermocline thickened in the subpolar site compared to the subtropical site for the same period. In contrast to MIS 6, a well-developed stratification at both sites was found during MIS 5e.

2. Geological and Oceanographic Setting

The principal sediments used in this study were collected by drilling on the Gardar Drift [33]. The modern observational data suggest that the westward-flowing Iceland–Scotland Overflow Water passes south of Iceland into the North Atlantic, significantly modifying Gardar Drift sediment sources [34,35]. The North Atlantic Current (NAC), the northeastern extension of the Gulf Stream, traverses northeastward between the subpolar

and subtropical gyres carrying a mixture of cold and fresh and warm and saline waters. The NAC splits into three sub-branches at around 50–52° N (Figure 1) after crossing the mid-Atlantic ridge [36]. The main NAC continues to flow into the northeast North Atlantic, passing the Iceland-Scotland Ridge into the Nordic seas [37]. A western-flowing branch of the NAC, the Irminger Current (IC), partly circulates Iceland and enters the Iceland Sea through the Denmark Strait, joins the East Greenland Current (EGC) at Cape Farwell and becomes part of the West Greenland Current (WGC). This current configuration of the surface currents in the NE Atlantic, including the Iceland Basin, is greatly influenced by the southward movement of the Polar and Arctic fronts during historical and past geologic periods [4,38–40].

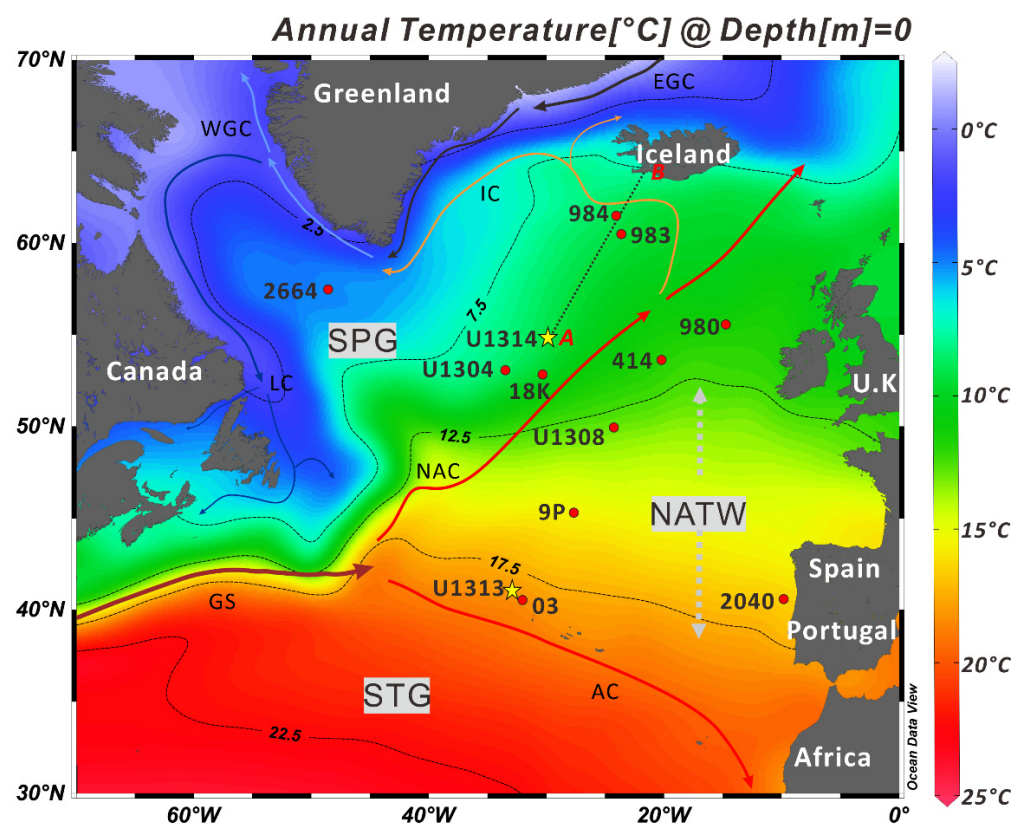


Figure 1. The location of cores discussed in the study is plotted. The approximate position of the North Atlantic Current (NAC), the northeastward extension of the Gulf Stream (GS), is shown by the thick red solid lines and arrows. Climatological data used to construct sea-surface temperature map were obtained from Locarnini et al. [38]. The Labrador Current (LC), West and East Greenland Currents (WGC and EGC), Irminger Current (IC), Flemish Cap (FC), and Azores Current (AC) paths are shown. The grey vertical arrow represents the approximate seasonal extent of the North Atlantic Transitional Water or Zone (NATW/Z). The black discontinuous line (A–B) exhibits the hydrographic transect illustrated in Figure 2. Note 2664 = MD03-2664; 18K = NEAP-18K; 03 = SU90-03; 9P = T90-9P; 414 = M23414; and 2040 = MD95-2040.

The physical oceanographic observational data suggest that the mean winter (January–March) and summer (July–September) sea-surface temperatures (SSTs) vary from 7.63 to 7.44 °C and 10.89 to 11.2 °C (Figure 2) [38], whereas the salinities range from 35.13–35.12 and 34.98–34.94 psu (practical salinity unit), respectively, surrounding IODP Site U1314. The well-established thermal structure is maintained at 6.5 °C at 400 m subsurface water depth. However, the isothermal layer between 7.5 and 6.5 °C (Figure 2a) crops out on the SW Iceland coast during winter. The 7.5 °C isothermal layer appears to shoal at 225 m (Figure 2c) at Site U1314 during summer. The high salinity layer off the coast of Iceland (Figure 2b) exhibits a wedge-shaped structure with a salinity of 35.20 psu extending as

far offshore [39] as Site U1314. This high salinity layer deepens to 1000 m during the summer (Figure 2d).

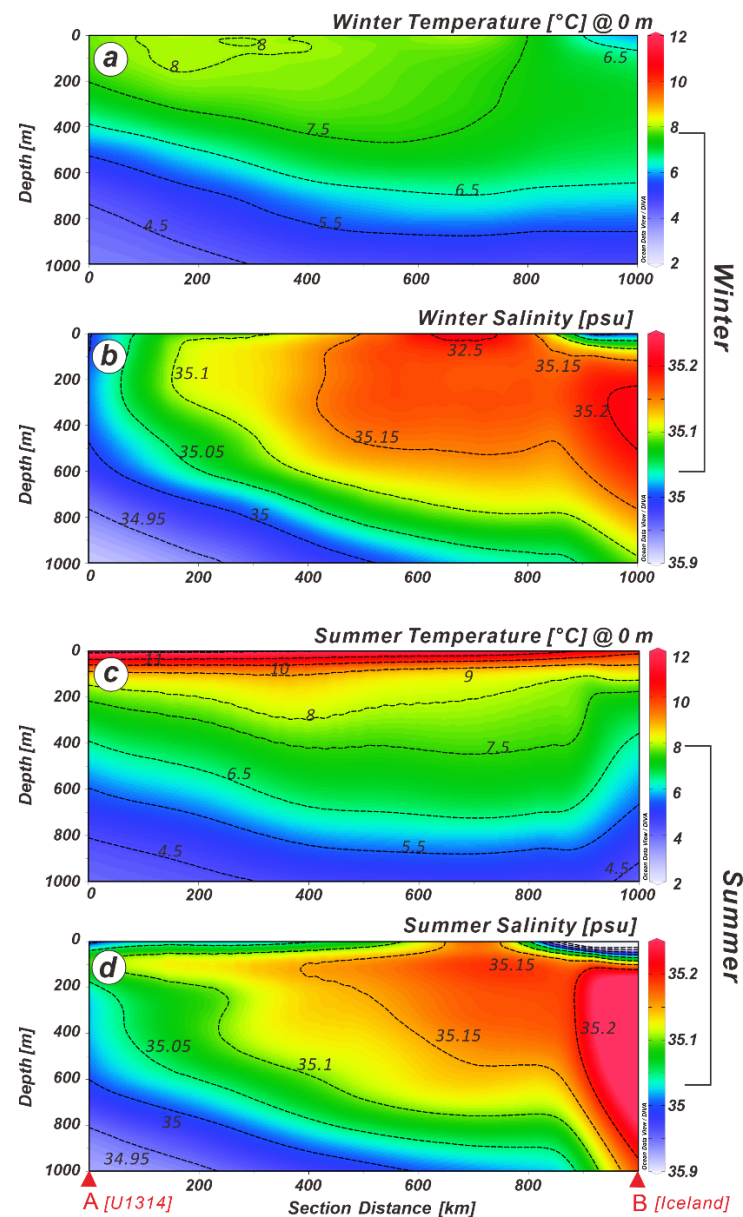


Figure 2. Modern winter and summer sea-surface temperature and salinity profiles stretch from the central North Atlantic to the western Icelandic continental margin (see Figure 1 for the location of the hydrographic transect). Seasonal deepening and shallowing of the thermocline are illustrated by (a,c), whereas the expansion and contraction of the low salinity layer in the Iceland Basin are shown by (b,d). Climatological data used to construct the hydrography were obtained from Locarnini et al. [38]. The map has been constructed by using Ocean Data View software [40].

3. Materials and Methods

During the 2005 IODP Expedition 306, Site U1314 was drilled on the southern Gardar Drift to retrieve sediments to study high-resolution changes in the sea-surface characteristics and North Atlantic Deep-Water formation during the Pleistocene [33,41]. Smith et al. [11] detailed Site U1313 (Figure 1).

The principal research materials used in the study were the sediment physical properties, bulk sediment geochemistry, and sediment samples collected by the IODP Expedition 306 at sites U1313 (41°00.6' N, 32°57.4' W; 3425 m water depth) and U1314 (56°21.9' N,

27°53.3' W; 2820 m water depth) in the North Atlantic (Figure 1). As part of the shipboard physical properties' measurement protocol, natural gamma rays (NGR) and sediment color (L^* , a^* , and b^*) were obtained at 2 cm intervals and were used in this study [33]. Using an Avaatech X-ray fluorescence (XRF) scanner at the Bremen Core Repository, University of Bremen (Germany), Gruetzner and Higgins [35] obtained bulk sediment geochemistry, namely Al, Si, K, Ca, Ti, and Fe concentrations from the Site U1314, which we used to ascertain key sediment intervals for identifying sediment facies and lithologic boundaries in this study (see below).

Samples from 10.00 to 15.18 and 5.65 to 9.15 m composite depth (mcd) from the IODP sites U1313 and U1314, respectively, were obtained at 10 cm intervals from the Bremen Core Repository. These samples were dried at 64 °C in an oven for 48 h and washed using a 63 μm brass sieve. The coarse fractions (i.e., 63 μm fractions) were sieved again at >150 μm fractions to count various planktonic foraminifers and ice-rafted debris (IRD). Approximately 300–600 foraminifers were counted to estimate the relative abundance of each species using a micro-splitter. By back-calculating the number of splits, the relative distribution of various species, including *Neogloboquadrina pachyderma*, *Neogloboquadrina incompta*, *Globigerina bulloides*, *Globorotalia inflata*, *Turborotalia quinqueloba*, etc. (see Rashid et al. [42], for details) were estimated. The dominant petrology of the IRD was also identified, in which a few detrital grains were tested using 10% hydrochloric acid under a binocular microscope. The identification of the detrital grains is especially important to trace Heinrich ice-rafting layers based on the presence of detrital carbonate grains [43,44].

Stable oxygen isotope ratios were determined on *G. bulloides* and *G. inflata* in a 150–250 μm size fraction for sites U1313 and U1314 in the Stable Isotope Biogeochemistry Laboratory at Ohio State University. The sampling frequency varies (*G. inflata* is absent in MIS 6 at Site U1314), but 62 and 28 samples were analyzed throughout the sites U1313 and U1314 intervals, respectively. Approximately twenty specimens of *G. bulloides* and *G. inflata* were picked to the required weight for mass spectrometer analysis and for future use in replicating isotopic results. It was ascertained that the combined weight of foraminifera in each sample was between 60 and 100 micrograms. Each sample was analyzed for $\delta^{18}\text{O}$ relative to NBS 18, 19, and 20 standards using an automated carbonate Kiel extraction device coupled to a Finnigan Delta IV Plus stable isotope ratio mass spectrometer at Ohio State University. Samples were acidified under vacuum with 100% ortho-phosphoric acid, the resulting CO_2 cryogenically purified, and delivered to the mass spectrometer. Approximately 10% of all samples were measured in duplicate. The standard deviation of repeated measurements of an internal standard was $\pm 0.06\text{‰}$ for $\delta^{18}\text{O}$ [42].

Gruetzner and Higgins [35] developed an age model by matching the wet-sediment color reflectance and magnetic susceptibility for Site U1314 to that of the ODP Site 983, which was drilled ~520 km northeast of Site U1314 and in ~1200 m shallower water [45]. Gruetzner and Higgins [35] transferred the age model of ODP Site 983 to Site U1314 to construct the age model for the last 1.1 Ma. We have fine-tuned the age model of Gruetzner and Higgins [35] between 10.15 and 15.18 mcd by obtaining oxygen isotopes in *G. bulloides*. The interval between 10 and 14.98 mcd covers sediment records from 114 to 199.40 ka, resulting in sedimentation rates from 11.4 to 13.31 cm/ka (Figure 3). The age model of Site U1313 for the last glacial cycle was reported by Smith et al. [11] and is therefore not detailed here. However, in brief, twenty tuning points were obtained by graphically matching the $\delta^{18}\text{O}$ of *G. bulloides* curve of Site U1313 to that of the benthic stack of Lisiecki and Raymo [46]. High and low $\delta^{18}\text{O}$ values were correlated to those of the high and low values of the global benthic stack (see Figure F1 of Smith et al. [11]). The sedimentation rates at Site U1313 vary from 4.66 to 5.17 cm/ka for the studied interval, slightly lower than those of Site U1314 but comparable to the published records of nearby cores [8,9].

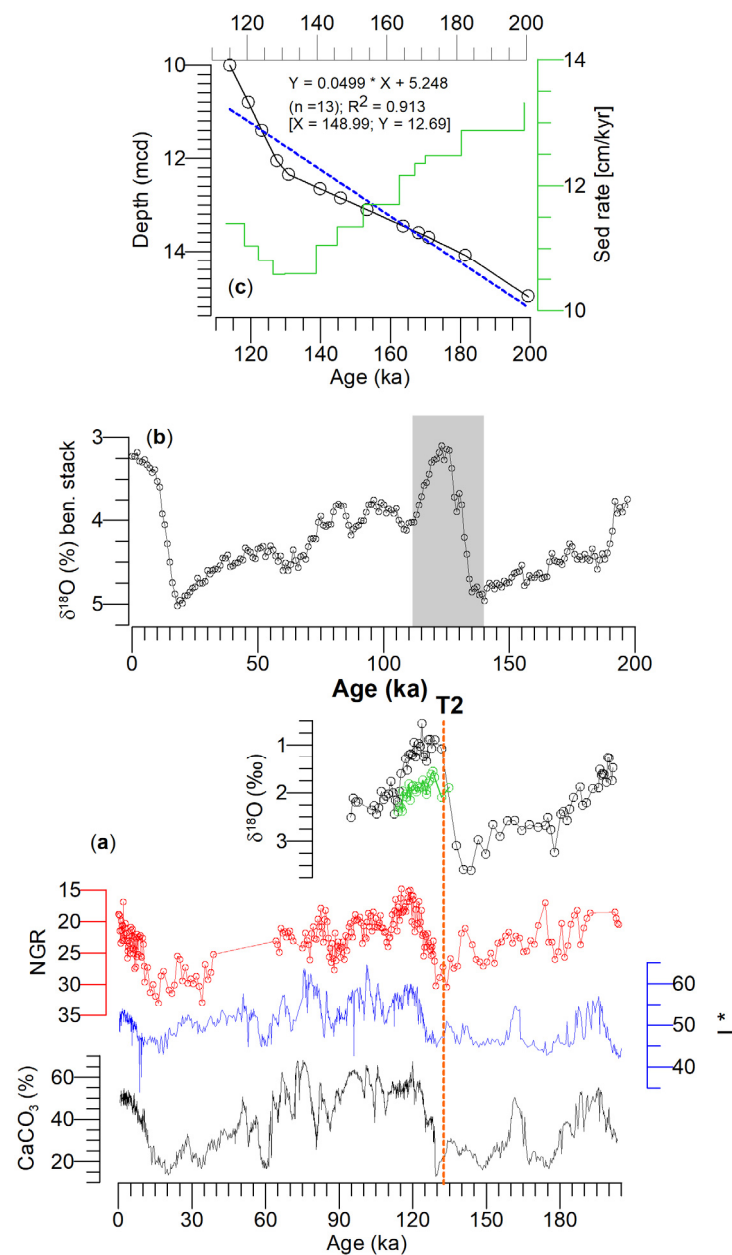


Figure 3. (a) (From bottom to top) estimated CaCO₃ (%) and color reflectance (L*) [35,47], natural gamma rays (NGR; reversed scale), and oxygen isotopes (δ¹⁸O) in *Globigerina bulloides* (black) and *Globorotalia inflata* (green) are plotted from the Site U1314 following the age model of Grützner and Higgins [35]. (b) Global benthic δ¹⁸O stack [46] was used to update the age model of Site U1314 by obtaining tie points with the δ¹⁸O in *Globigerina bulloides* between 10 and 15.20 mcd shown in (c). The vertical orange discontinuous line in (a) represents Termination 2 (T2).

4. Results

• Site U1314

The δ¹⁸O curve of *G. bulloides* shows a typical deglacial sequence with enriched values in glacial MIS 6, and depleted values in MIS 5e at IODP site U1314 (Figure 4). The abrupt change in δ¹⁸O values between the isotope stages is identified as T2. The depleted δ¹⁸O values of *G. inflata* reflect warmer interglacial MIS 5e [27]. No *G. inflata* were found within the MIS 6, thus preventing us from reconstructing an isotopic curve for *G. inflata* in this interval. In MIS 5e, *G. bulloides* shows more depleted δ¹⁸O values compared to *G. inflata* (Figure 4).

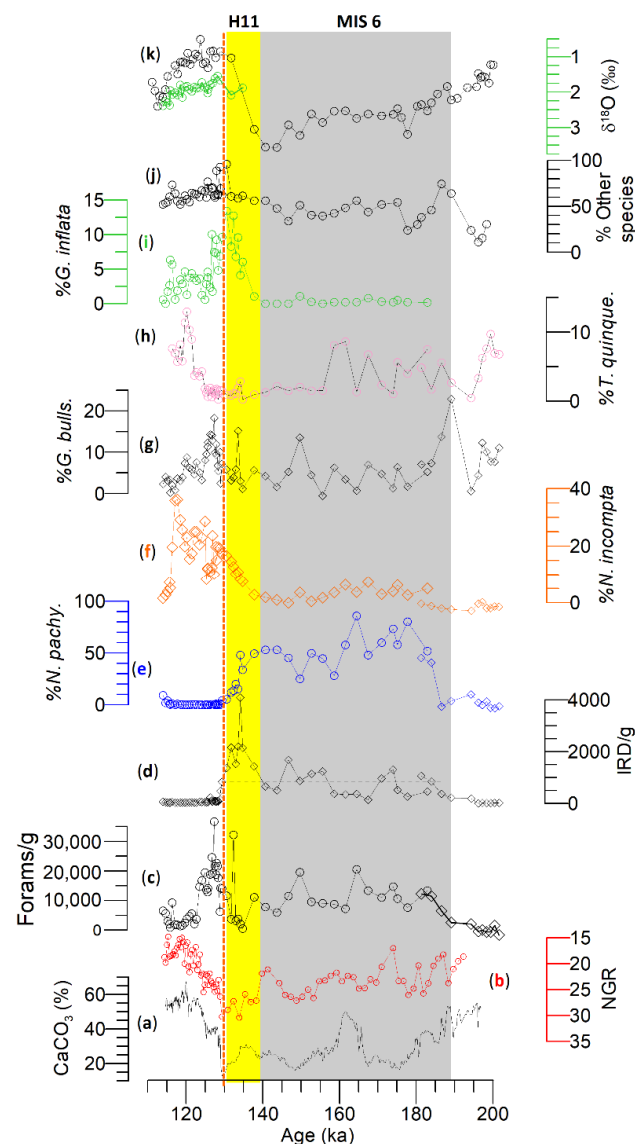


Figure 4. (a) Estimated CaCO_3 (%), (b) natural gamma radiation (NGR; reverse scale); (c) foraminifers/g of dry sediments, (d) ice-rafted debris (IRD)/g of dry sediments, (e–i) % *N. pachyderma*, *N. incompta*, *G. bulloides*, *T. quinqueloba*, *G. inflata*, and (j) “other species” are plotted from the Site U1314. (k) $\delta^{18}\text{O}$ in *G. bulloides* (black) and *G. inflata* (green). The vertical yellow and grey bars highlight Heinrich event 11 and MIS 6, respectively. Note horizontal discontinuous bar in (d) represents the mean IRD/g concentration between 192.41 and 126.22 ka, whereas the orange vertical line represents T2.

The percent *N. pachyderma* (Figure 4e) displays a general glacial-interglacial trend by inversely following the *G. bulloides* $\delta^{18}\text{O}$ curve (Figure 4j). The overall percentage of *N. pachyderma* is sustained at high levels during MIS 6 and gradually decreases throughout the penultimate deglaciation. The abundance of *N. pachyderma* greatly diminishes in the interglacial and almost disappears during MIS 5e. *G. bulloides* (Figure 4g) exhibits a more variable abundance trend but is present throughout both stages. It maintained a robust abundance peak during the early phase of MIS 5e, reaching over 15%. *G. bulloides* abundance increases during the deglaciation gradually and is generally inversely correlated with *N. pachyderma*. *G. inflata* (Figure 4i) remains nearly absent throughout MIS 6. It reached a maximum abundance of 15% at the end of H11 and remained in higher abundance in early MIS 5. It averages around 5% abundance in the latter phase of MIS 5. *N. incompta* (Figure 4f) also displays a general glacial-interglacial trend. The abundances of *N. incompta* increased rapidly during the T2, with the highest concentrations

of 30% occurring in late MIS 5. *N. incompta* is nearly absent in MIS 6 when *N. pachyderma* is at its highest abundance. Thus, these two species are generally inversely correlated with each other. There is a corresponding abundance decrease in *G. bulloides* and *N. incompta* at 127.27 ka (Figure 4); however, *N. pachyderma* remains nearly absent, showing no change.

IRD/g (Figure 4d) at Site U1314 exhibits very high concentrations throughout MIS 6, and high IRD peaks correspond to high abundance of *N. pachyderma*. The IRD peak increases sharply halfway through glacial T2, then decreases abruptly before leveling off in MIS 5e, where only trace IRD exists. The IRD maximum is tentatively correlated to Heinrich event 11 (H11) but needs verification.

- *Site U1313*

Planktonic foraminiferal assemblages and IRD abundance, in addition to the $\delta^{18}\text{O}$ of *G. bulloides* of Site U1313, are detailed by Smith et al. [10] and are also plotted in Figure 5. However, the $\delta^{18}\text{O}$ in *G. inflata* is reported here for the first time. In any case, the $\delta^{18}\text{O}$ *G. inflata* curve follows $\delta^{18}\text{O}$ *G. bulloides* values during MIS 6 and T2 with a minor offset (Figure 5) in which the former always exhibits lighter values compared to the latter. However, the $\delta^{18}\text{O}$ *G. inflata* shows slightly enriched values compared to the $\delta^{18}\text{O}$ *G. bulloides* between 127 and 115 ka (Figure 5).

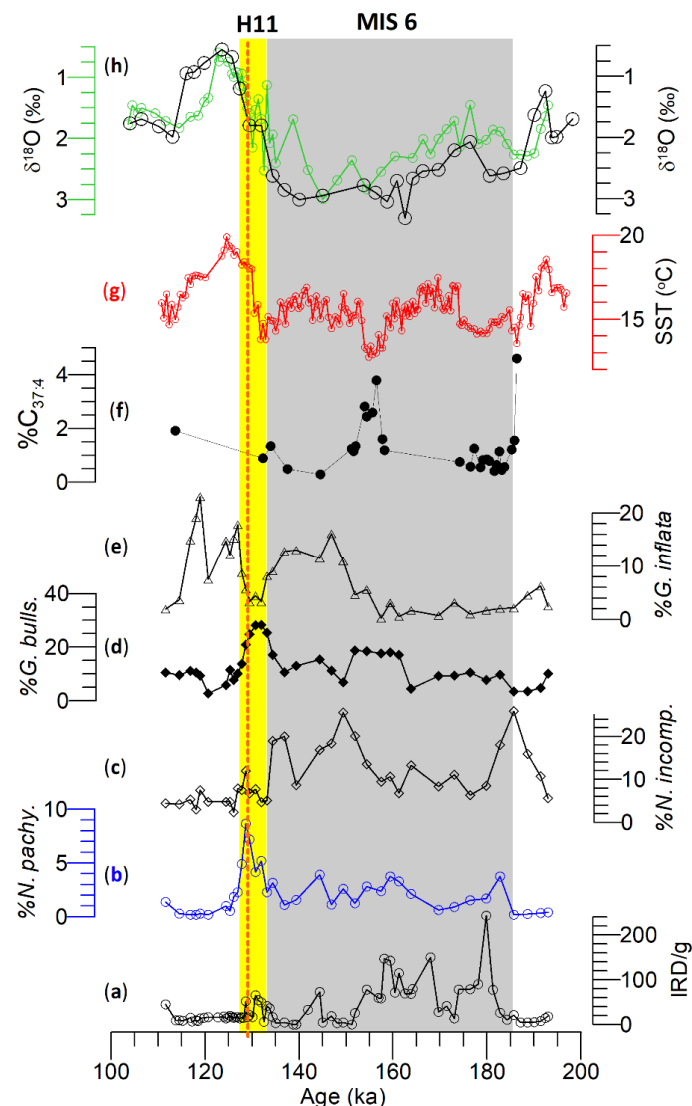


Figure 5. Various attributes of Site U1313. (a) ice-rafted debris (IRD)/g, (b–e) % *N. pachyderma*, *N. incompta*, *G. bulloides*, and *G. inflata*, according to Smith et al. [11]. (f,g) %C_{37:4} and alkenone-based

SST (°C) [10]. (h) $\delta^{18}\text{O}$ in *G. bulloides* (black) and *G. inflata* (green) are plotted following the age model of Smith et al. [11]. H11 is highlighted by the vertical yellow bar, whereas the grey vertical bar indicates MIS 6. H11 coincides with a peak in *G. bulloides* and a low abundance of *G. inflata*. The discontinuous orange line depicts Termination 2 (T2).

5. Discussion

5.1. Subpolar to Subtropical Water Mass Movement during MIS 6

Paleo-proxy records from IODP sites U1313 and U1314 allow us to reconstruct the evolution of subpolar to subtropical gyre sea-surface conditions from the penultimate glaciation to deglaciation. Moreover, the published data from the ODP/IODP sites U1304 [25], U1308 [48], 983 [49], 984 [4], and piston cores M23414 [7] and MD95-2040 [50] afford us to place data from this study into a broader perspective. In any case, the $\delta^{18}\text{O}$ in *G. bulloides* shows progressive enrichment in MIS 6 (i.e., between 195 and 140 ka) and smooth deglacial transition from MIS 6 to 5 (Figure 4) at Site U1314. These climate records are consistent with reports from the nearby core M23414 [7] and Site U1308 [48] and the sites 983 [49] and 984 [4] and Site U1304 [25] of the northeastern subpolar gyre in the south of Iceland.

The subpolar climate at Site U1314: Occasional minor IRD peaks (Figure 4) imply iceberg rafting by the Icelandic and Irish-British ice sheets, consistent with the earlier findings from the same site [47] and other eastern subpolar records [49,51]. However, the high IRD peak (132–129 ka) correlates to the Laurentide ice sheet (LIS) sourced [3,52] H11 of the North Atlantic, implying that it might have originated from the LIS; however, petrological data are needed to confirm its provenance. Surprisingly, Hodell et al. [25] reported a near 0% CaCO_3 which the authors identified as H11 without providing IRD data at Site U1304, raising questions about the veracity of the identification of H11. Mokeddem and McManus [4] reported a high-resolution IRD record from ODP Site 984 compared to the earlier coarse-resolution data from the nearby ODP Site 980 on the Feni Drift [3]. The authors identified low-magnitude IRD peaks that lacked the detrital carbonate supporting the hypothesis of lack of massive ice-rafting with IRD on the greater NE Atlantic during MIS 6 [4,49]. Farther south on the subtropical Portuguese margin, deAbreau et al. [50] identified a few considerably low-concentration IRD peaks from core MD95-2040, nearly identical to the IRD peaks identified at ODP sites 980 and 984. Those minor IRD peaks comprise angular quartz grains and volcanic particles compared to the detrital carbonate grains in H-events of the North Atlantic [48,52,53]. These IRD records suggest that iceberg discharge was far less pronounced during MIS 6 compared to MIS 3 [5,15,48]. Further, the lack of detrital carbonate grains in the IRD/g peaks suggests a far more stable LIS during MIS 6 [42,54,55]. The presence of quartz grains and volcanic particles implies the contribution of icebergs by the Icelandic and Irish-British ice sheets at this time as well [56,57]. In any case, the discharge of icebergs had a significant impact on the surface hydrography on the greater Iberian margin. For example, Margari et al. [58] reported lighter $\delta^{18}\text{O}$, which the authors attributed to freshwater originating from icebergs without IRD [50]. However, whether the freshwaters were derived from the western European discharge [51] or by iceberg melting is unknown due to the lack of IRD/g data from the same margin. No significant lighter $\delta^{18}\text{O}$ values at Site U1314 suggest a regional heterogeneity on the surface hydrography by the freshwater. It is plausible that the prevailing colder sea surface temperature canceled the impact of freshwater, but that proposition is unlikely due to the lack of significant IRD peaks in MIS 6 (Figure 4). It may also suggest that the freshwaters were carried by the southward-flowing Portugal Current, impacting only the surface hydrography of the Portuguese margin during MIS 6 [58].

The high *N. pachyderma* concentration between 190 and 132.5 ka (Figure 4) suggests an incursion by the Arctic and polar waters, implying that the Arctic and Polar fronts were south of Site U1314. While the occasional presence of *G. bulloides* indicates a short seasonal transitional water intrusion by the NAC during late spring or early summer (Figure 4). Further, the MIS 6 period could be divided into two periods (190–160 and 160 and 135 ka) based on % *N. pachyderma* at Site U1314. The concentration of *T. quinqueloba*, a subpolar

water mass indicator at Site 984 [4] and northeastern subpolar gyre [59], seems to loosely covary with the % *N. pachyderma*, although the relative concentration of the former is insignificant. In any case, the trace of *G. inflata*, *N. incompta*, and *T. quinqueloba* [60–62] further support the presence of a prevailing cold climate regardless of the season during MIS 6. Using mostly *N. pachyderma* and other foraminiferal concentrations at ODP Site 984, Mokeddem and McManus [4] reported three interstadial events centered at 163, 152, and 146 ka within MIS 6 in which only the interstadial event centered at 152 ka exhibits a minor *T. quinqueloba* rise. The authors reasoned these interstadial events were due to the invasion by the subpolar water (Arctic front) at the expense of the Polar waters [59]. Therefore, the differences in IRD peaks and foraminiferal assemblages between sites 984 and U1314 most likely reflect regional heterogeneity in which the former site (i.e., 984) was under the complete influence of the Polar front [49]. In contrast, the relatively southern Site U1314, located within the NATW/Z, was seasonally influenced by the NAC, notwithstanding the dominance of the Arctic and polar waters.

In contrast to the subpolar sites 984 and U1314, sea-surface conditions around the region of core M23414 (Figure S1), located in the NATW/Z at present (Figure 1), were different, indicated by the foraminiferal assemblage, IRD/g, and planktonic foraminiferal oxygen isotopes [63]. For example, the *N. pachyderma* concentration between Site U1314 and M23414 is anticorrelated as such high and low *N. pachyderma* from 185 to 162 ka and 160 to 135 ka at Site U1314 with the low and high *N. pachyderma* at M23414. Further, high *T. quinqueloba* and *N. pachyderma* from 185 to 162 ka correlate to low *N. pachyderma* at M23414. Such an anticorrelation among the foraminiferal species is non-existent at Site U1314, most likely due to the predominance of polar and subpolar waters, reflecting the Polar and Arctic frontal movements. In contrast to Site U1314, the variable changes in the planktonic foraminiferal assemblages suggest a dynamic turnover of the polar and subpolar water masses in the NATW/Z around the region of core M23414. The near absence of *G. inflata*, a temperate water mass indicator (~8–18 °C) associated with the NAC in the NE Atlantic [64,65], at sites U1304 [25] and U1314 and core M23414, further corroborates the dominance by the polar and subpolar water masses at these sites during MIS 6. Billups et al. [66] suggested compression of the subtropical gyre due to the southward advancement of the Polar and Arctic fronts during glacial times; however, the extent to which such a physical mechanism operated at Site U1313 cannot be assessed due simply to the lack of *Globorotalia truncatulinoides* (sinistral) data for MIS 6 period.

The subtropical gyre boundary record at Site U1313: The $\delta^{18}\text{O}$ curves of *G. bulloides* and *G. inflata* exhibit enriched values throughout MIS 6 compared to MIS 5 (Figure 5) at the subtropical Site U1313. A relatively lighter $\delta^{18}\text{O}$ in *G. bulloides* and *G. inflata* centered at 175 ka most likely suggests a brief warm water incursion by the NAC. A clear lack of IRD peaks and the associated presence of icebergs, which would have freshened the sea surface, supports this proposition. This hypothesis is further supported by alkenone-based SSTs and tetra-bond $\%C_{37:4}$ (Figure 5) from the same site [10]. One of the important observations is the nearly identical (or even slightly lighter $\delta^{18}\text{O}$ in *G. inflata*) $\delta^{18}\text{O}$ values between the mixed-layer species *G. bulloides* and thermocline dwelling *G. inflata* during the MIS 6 compared to MIS 5 (Figure 5). *G. bulloides* is primarily associated with subpolar to temperate regions [67,68] and reflects sea-surface and productivity conditions during late spring to summer in the subpolar region [69]. Schiebel et al. [70] suggested that the preferential depth habitat of *G. bulloides* varies from living in or above the thermocline (i.e., restricted to 60 m or shallower) in the NE Atlantic. In contrast to *G. bulloides*, past studies suggest that *G. inflata* is most abundant in temperate waters but also ranges to subpolar and subtropical water masses and is associated with the NAC [8,9,71]. *G. inflata* is deep-dwelling species associated with the base of the thermocline [64], which would be at 100 m or slightly deeper around Site U1313 [38,72]. Therefore, the near identical $\delta^{18}\text{O}$ values in *G. bulloides* and *G. inflata* suggest seasonal mixed layer and thermocline records at Site U1313 during MIS 6. It could be argued that the seasonal transitional water masses (a mixer of subpolar and relatively warmer NAC due to enhanced wind stress) might produce

identical $\delta^{18}\text{O}$ values [15]. The extent to which factors (i.e., temperature and low $\delta^{18}\text{O}$ freshwater) dominated in producing identical $\delta^{18}\text{O}$ values cannot be separated at present as the independent temperature (e.g., Mg/Ca ratios) data at Site U1313 are unavailable.

Mulitza et al. [73] proposed a “water column stratification” index in which similar $\delta^{18}\text{O}$ ($\Delta\delta^{18}\text{O}$: 0; $\delta^{18}\text{O}_{\text{Gb}} - \delta^{18}\text{O}_{\text{Ginf.}}$) of *G. bulloides* and *G. inflata* suggest a well-mixed water column, i.e., a homogenized mixed layer and thermocline. If the “water column stratification” index is applied to the $\delta^{18}\text{O}$ values in MIS 6 at Site U1313, it suggests that a mixed water column without a thermocline prevailed [74]. Mokedem and McManus [4] have suggested stratification of the upper water column using *N. pachyderma* and *N. incompta* from ODP Site 984 during MIS 6 as well. It is postulated that the lack of water column stratification has weakened the heat transport by the NAC during MIS 6. The abundance decreases in *G. inflata* and alkenone-based SST data [10] appear to support this hypothesis.

Four IRD/g (Figure 5) peaks composed of quartz, igneous, and metamorphic rock fragments were identified but lacked detrital carbonate grains at Site U1313 [11], suggesting European and east Greenland ice sheet sources [53]. These IRD peaks do not accompany any concomitant lighter $\delta^{18}\text{O}$ (Figure 5), implying their limited impact on sea-surface freshening. However, these IRD peaks tentatively match the four depleted $\delta^{18}\text{O}$ values in *G. bulloides* on the Portuguese margin [58]. The abundance of *N. pachyderma* does not rise above 2.5%, consistent with the identical *N. pachyderma* concentration during the last glacial maximum [9], suggesting a prevailing temperate climate during MIS 6. *G. inflata* exists in low abundance at Site U1313 throughout MIS 6 owing to plausibly warmer southern latitudes as opposed to its complete absence at Site U1314 at the same time. Two millennial-scale transitional water mass events were reflected by two *N. incompta* peaks centered at 185.68 and 149.38 ka (Figure 5). Brief subpolar water traversed Site U1313 during the latter part of MIS 6. One of the interesting anticorrelations was determined between *N. pachyderma* and *G. bulloides*/*G. inflata* at sites U1314 and U1313, where the percent of *N. pachyderma* is high at Site U1314, the percent of *G. bulloides*/*G. inflata* is low at Site U1313 during the earlier part of MIS 6 (185–160 ka). This correlation reverses during the latter part of MIS 6 (160–140 ka) and likely reflects the presence of the Polar front at Site U1314 while the transitional water masses (NAC) incurred at Site U1313.

In summary, Site U1314 contains a higher IRD/g compared to Site U1313, although these sites are located north and south of the IRD-belt [23], respectively, reflecting the importance of the geographic location in assessing the ice sheets' instability. Site U1313 displays a higher diversity of planktonic foraminifers with lower abundances, whereas Site U1314 reflects low diversity and a dominated assemblage during MIS 6. The much higher abundance of *N. pachyderma* at Site U1314 reflects the prevalence of polar and subpolar water masses. The very low abundance of the other species indicates a stressful environment suggesting that sea-surface conditions were too cold for other species. The subtropical location of Site U1313 is normally unsuitable for *N. pachyderma* [75,76], but the glacial conditions created a suitable environment for the subpolar and transitional water species [32,77].

5.2. Subpolar-Subtropical Surface Water Masses Transformation during T2 and MIS 5e

The $\delta^{18}\text{O}$ curves at T2 reflect a rapid transition at the subpolar Site U1314 but a more gradual transition at the subtropical Site U1313, suggesting a differential response to water masses by the sea-surface conditions. The lack of adequate specimens of *G. inflata* prevented us from obtaining an equivalent number of isotopic measurements compared to *G. bulloides* at Site U1314 during T2 (Figure 4), but both species were present at Site U1304 [25]. Moreover, the $\delta^{18}\text{O}$ *G. inflata* and *G. bulloides* curves follow each other at Site U1313 during T2 (Figure 5), like at Site U1304 [25], reflecting a regional homogeneity in sea-surface temperature and surface water masses during T2. In contrast to distinct $\delta^{18}\text{O}$ values of *G. inflata* and *G. bulloides* at Site U1313 during MIS 6 (Figure 5), the $\delta^{18}\text{O}$ curves in both species exhibit depletion and identical values (Figures 4 and 5) immediately after the T2 during MIS 5e. The near identical *G. bulloides* and *G. inflata* $\delta^{18}\text{O}$ values during T2 at Site

U1313 suggest a well-mixed water column when the water column stratification index of Mulitza et al. [73] is applied. The negative $\Delta\delta^{18}\text{O}$ values suggest the re-establishment of water column stratification during MIS 5e (Figure 5), indicating the presence of a seasonal (spring-summer) thermocline at both sites. One of the implications of the stratified water column is strengthening the NAC, thus, bringing warmer transitional waters from low latitudes near identical conditions prevailing today [37]. The sudden increase in the abundance of *G. inflata* provides further support to this proposition.

Heinrich event 11 (Figures 4 and 5), which punctuated the penultimate deglaciation, was identified by a prominent IRD peak at Site U1314, but it is subdued (i.e., lower magnitude) at Site U1313. Further, a differential response in the surface water masses between the sites reflects the state (i.e., thinner versus thicker) of the mixed layer and thermocline, as well as the seasonality. For example, a prominent *N. pachyderma* peak is concomitant with H11 at Site U1313, but no distinct change at Site U1314, consistent with the earlier report from the nearby core NEAP-18K [78]. It is noteworthy that warmer sea-surface conditions are normally unsuitable for *N. pachyderma* to thrive at Site U1313 [79,80]. The meltwater released by icebergs during H11 most likely cooled the sea surface at Site U1313 but inadequately cold to attain a concentration of *N. pachyderma* (i.e., 10%) as high as during H-events [22,42,50], consistent with the near-identical concentration reported in earlier studies [8,9]. The low *N. pachyderma* percent suggests the brief presence of seasonal subpolar water masses at Site U1313, consistent with the slight cooling in alkenone-based SSTs [10]. Further east across the mid-latitude North Atlantic at site MD95-2040, deAbreu et al. [50] reported subpolar species increase and subtropical species decrease, suggesting an incursion by the cold Portuguese Current on the Iberian margin. The sea-surface cooling is also recorded by the alkenone data on the same margin, but not all cooling events were associated with the freshwater arrival (i.e., % $\text{C}_{37:4}$) [81]. This difference between the cooler SSTs and % $\text{C}_{37:4}$ may explain some of the dichotomies among paleo-proxies at Site U1313 (Figure 5). In contrast to Site U1313, sea-surface conditions at Site U1314 were cooler, and *N. pachyderma* flourished during the glacial period reaching a peak abundance of nearly 80% during MIS 6. Site U1314 is relatively cooler due to its location in the subpolar gyre [33,45]; thus, the freshwater incursion most likely did not cool the sea surface enough to usher an equitable polar environment suitable for dominance by *N. pachyderma* [82,83], resulting in an insignificant increase during H11.

G. bulloides demonstrates a different response to each IODP site. Site U1313 exhibits a prominent abundance peak during H11, consistent with the concentration in core SU90-03 [9], reflecting sea-surface cooling by the freshwater conditioning seasonal subpolar environment in the subtropics [74], whereas the absence of a *G. bulloides* peak at Site U1314 suggests Arctic water incursion. A similar increase in *G. bulloides* was also reported from the nearby core T90-9P [28]. However, the abundance of *G. bulloides* decreases during the interglacial (MIS 5e) at Site U1313, and a contemporaneous increase in shell fragments [21] due to changes in the bottom water chemistry, which usually increases shell fragmentation may account for this. During early MIS 6 and H11, the poor abundance of *G. inflata* demonstrates that it diminishes with colder conditions at Site U1313. The higher *G. bulloides* abundances at Site U1314 suggest its preference for warmer and better productivity conditions [22,64] during the interglacial (MIS 5e). During the warmest part of MIS 5e, the abundances of *N. pachyderma* decrease to a trace amount, whereas *N. incompta* increases, suggesting seasonal penetration by the warm NAC at Site U1314, consistent with the data in core MD03-2664 [22]. The abundance of *N. incompta* is inversely correlated with *N. pachyderma* (Figures 4 and 5). During peak intervals, the absolute percentage of *N. incompta* reaches only about half that of *N. pachyderma*. Further, *N. incompta* follows the $\delta^{18}\text{O}$ in *G. bulloides*, whereas *N. pachyderma* shows an inverse correlation suggesting the presence of the seasonal transitional (NAC) environment. At the end of T2, peak *G. inflata* abundance suggests that the warm NAC penetrated to high latitudes (Figure 4). Our data suggest a complex but rapid interplay of colder versus warmer waters at Site U1314.

The negative $\Delta\delta^{18}\text{O}$ values (Figures 4 and 5) at both sites suggest the re-establishment of the mixed layer and thermocline during MIS 5e. The arrival of warmer subpolar and transitional waters at Site U1314 is evidenced by the absence of *N. pachyderma* and by the increase in *G. inflata* [84]. In contrast to Site U1314, the immediate rise in *N. incompta* suggests the arrival of warm transitional water masses borne by the NAC at the ODP Site 984 [4]. Moreover, the anticorrelation between *N. incompta* and *T. quinqueloba* from 131 to 115 ka (Figure 4) suggests a gradual retreat of the NAC at the expense of the subpolar water, due most likely to the southward migration of the Arctic front [59]. Kandiano et al. [63] have reported a near-identical increase in *N. incompta* and *G. inflata*, but an absence of a rise in *G. bulloides* from core M23414 affirmed the intensification of the transitional water masses. The increase in *N. incompta* was compensated by the decrease in *G. bulloides* from the onset of T2 to throughout MIS 5e (Figure 4). The increase in *G. bulloides*, *G. inflata*, and *N. incompta* in MIS 5e suggests a return of warmer surface conditions, as these species are usually associated with the NAC at Site U1314. In MIS 5e, a higher diversity of species with lower abundances was found at Site U1314. At the warmest point of MIS 5e at Site U1313, *G. inflata* decreased, and *G. bulloides* reached a maximum suggesting a strong subpolar to transitional water inflow. In contrast, *G. inflata* dominates the assemblage (Figure 5) during MIS 5e owing to much warmer surface conditions suggesting a stronger influence by the NAC.

In summary, a decrease in *N. pachyderma* was compensated by the dominance of *G. inflata* immediately after the H11, suggesting a rapid turnover of the sea-surface conditions at subpolar Site U1314. At Site U1313, the return of *N. pachyderma* immediately after H11 indicates a prevailing cooler sea-surface condition. *G. bulloides* exhibits a prominent peak during H11 at Site U1313 but poor abundances at Site U1314.

6. Conclusions

We have reconstructed changes in the mixed layer and thermocline and their mixing from MIS 6 to MIS 5e at IODP sites U1313 and U1314, which are currently located in the subtropical and subpolar gyre of the North Atlantic. Our findings are briefly listed below.

- (i). During MIS 6, four low amplitude IRD peaks were identified where the IRD peaks at Site U1314 were higher than that of Site U1313. *N. pachyderma* is dominant at Site U1314, reflecting the prevailing presence of polar and subpolar water masses. The diversity of planktonic foraminifers at the STG Site U1313 is higher than that of subpolar Site U1314 in addition to subpolar and transitional species alongside significant changes in *N. pachyderma*. These changes in the foraminiferal assemblages reflect the evolution of the North Atlantic transitional water and subpolar water masses.
- (ii). During MIS 6, the $\delta^{18}\text{O}$ of *G. bulloides* and *G. inflata* is nearly identical at Site U1313, most likely caused by the seasonal incursion of transitional water masses resulting in seasonal blooms of each species dwelling in their respective depth habitats. However, this proposition requires examination by isolating temperature from the $\delta^{18}\text{O}$ in both species.
- (iii). Planktonic foraminifera $\delta^{18}\text{O}$ values at sites U1313 and U1314 during T2 reflect regional heterogeneity of transition from penultimate deglacial to interglacial time. It appears that the transition speed at Site U1314 was fast compared to Site U1313. Further, the identical $\delta^{18}\text{O}$ values of *G. bulloides* and *G. inflata* at Site U1313 reflect a well-mixed water column during T2.
- (iv). Negative $\Delta\delta^{18}\text{O}$ ($\delta^{18}\text{O}_{\text{Cb}} - \delta^{18}\text{O}_{\text{Ginf.}}$) values between sites U1313 and U1314 reflect the re-establishment of the water column (i.e., mixed layer and thermocline) during MIS 5e. The *N. incompta* increase at Site U1314, and the increase in *G. inflata* at Site U1313 reflects the influence of warm NAC during MIS 5e.

Supplementary Materials: The following are available online at <https://www.mdpi.com/article/10.3390/geosciences13050149/s1>, Figure S1: Core M23414.

Author Contributions: Conceptualization, H.R.; methodology, H.R.; validation, M.Z. and M.M.; formal analysis, J.C.; investigation, J.C. and M.Z.; resources, H.R.; data curation, J.C. and M.M.; writing—original draft preparation, H.R. and J.C.; writing—review and editing, M.M., J.C. and M.Z.; visualization, J.C.; supervision, H.R.; project administration, H.R.; funding acquisition, H.R. All authors have read and agreed to the published version of the manuscript.

Funding: This research was funded by the National Natural Science Foundation of China, grant numbers 41976056 and 41776064.

Data Availability Statement: Data used in this article are archived at http://ed/nrcan.gc.ca/index_e.php (accessed on 25 October 2022) and are freely available.

Acknowledgments: Part of the study was conducted when the senior author was supported by the Byrd Polar Climate and Research Center Fellowship. B. Rodgers, S. Lodestro, and E. England are acknowledged for their help in processing sediment samples. MEM acknowledges the support from Shell through an internship. The Integrated Ocean Drilling Program provided samples for this study.

Conflicts of Interest: The authors declare no conflict of interest.

References

1. Svendsen, J.I.; Alexanderson, H.; Astakhov, V.I.; Demidov, I.; Dowdeswell, J.A.; Funder, S.; Gataullin, V.; Henriksen, M.; Hjort, C.; Houmark-Nielsen, M.; et al. Late Quaternary Ice Sheet History of Northern Eurasia. *Quat. Sci. Rev.* **2004**, *23*, 1229–1271. [[CrossRef](#)]
2. Jakobsson, M.; Nilsson, J.; O'Regan, M.; Backman, J.; Löwemark, L.; Dowdeswell, J.A.; Mayer, L.; Polyak, L.; Colleoni, F.; Anderson, L.G.; et al. An Arctic Ocean Ice Shelf during MIS 6 Constrained by New Geophysical and Geological Data. *Quat. Sci. Rev.* **2010**, *29*, 3505–3517. [[CrossRef](#)]
3. McManus, J.F.; Oppo, D.W.; Cullen, J.L. A 0.5-Million-Year Record of Millennial-Scale Climate Variability in the North Atlantic. *Science* **1999**, *283*, 971–975. [[CrossRef](#)]
4. Mokeddem, Z.; McManus, J.F. Persistent Climatic and Oceanographic Oscillations in the Subpolar North Atlantic during the MIS 6 Glaciation and MIS 5 Interglacial. *Paleoceanography* **2016**, *31*, 758–778. [[CrossRef](#)]
5. Bond, G.; Broecker, W.; Johnsen, S.; McManus, J.; Labeyrie, L.; Jouzel, J.; Bonani, G. Correlations between Climate Records from North Atlantic Sediments and Greenland Ice. *Nature* **1993**, *365*, 143–147. [[CrossRef](#)]
6. McManus, J.F.; Bond, G.C.; Broecker, W.S.; Johnsen, S.; Labeyrie, L.; Higgins, S. High-Resolution Climate Records from the North Atlantic during the Last Interglacial. *Nature* **1994**, *371*, 326–329. [[CrossRef](#)]
7. Kandiano, E.S.; Bauch, H.A. Surface Ocean Temperatures in the North-East Atlantic during the Last 500 000 Years: Evidence from Foraminiferal Census Data: Surface Ocean Temperatures in the North-East Atlantic. *Terra Nova* **2003**, *15*, 265–271. [[CrossRef](#)]
8. Ruddiman, W.F.; Raymo, M.E.; Martinson, D.G.; Clement, B.M.; Backman, J. Pleistocene Evolution: Northern Hemisphere Ice Sheets and North Atlantic Ocean. *Paleoceanography* **1989**, *4*, 353–412. [[CrossRef](#)]
9. Chapman, M.R.; Shackleton, N.J.; Duplessy, J.-C. Sea Surface Temperature Variability during the Last Glacial–Interglacial Cycle: Assessing the Magnitude and Pattern of Climate Change in the North Atlantic. *Palaeogeogr. Palaeoclimatol. Palaeoecol.* **2000**, *157*, 1–25. [[CrossRef](#)]
10. Naafs, B.D.A.; Hefter, J.; Stein, R. Millennial-Scale Ice Rafting Events and Hudson Strait Heinrich(-like) Events during the Late Pliocene and Pleistocene: A Review. *Quat. Sci. Rev.* **2013**, *80*, 1–28. [[CrossRef](#)]
11. Smith, M.; Glick, E.; Lodestro, S.; Rashid, H. Data Report: Oxygen Isotopes and Foraminifer Abundance Record for the Last Glacial–Interglacial Cycle and Marine Isotope Stage 6 at IODP Site U1313. In *Expedition 303/306 Scientists*; Channell, J.E.T., Kanamatsu, T., Sato, T., Stein, R., Alvarez Zarikian, C.A., Malone, M.J., Eds.; Integrated Ocean Drilling Program Management International, Inc.: College Station, TX, USA, 2013; Volume 303/306.
12. Cheng, H.; Edwards, R.L.; Broecker, W.S.; Denton, G.H.; Kong, X.; Wang, Y.; Zhang, R.; Wang, X. Ice Age Terminations. *Science* **2009**, *326*, 248–252. [[CrossRef](#)] [[PubMed](#)]
13. Ruddiman, W.F.; McIntyre, A. Oceanic Mechanisms for Amplification of the 23,000-Year Ice-Volume Cycle. *Science* **1981**, *212*, 617–627. [[CrossRef](#)] [[PubMed](#)]
14. Sarnthein, M.; Winn, K.; Jung, S.J.A.; Duplessy, J.-C.; Labeyrie, L.; Erlenkeuser, H.; Ganssen, G. Changes in East Atlantic Deepwater Circulation over the Last 30,000 Years: Eight Time Slice Reconstructions. *Paleoceanography* **1994**, *9*, 209–267. [[CrossRef](#)]
15. Rashid, H.; Boyle, E.A. Mixed-Layer Deepening During Heinrich Events: A Multi-Planktonic Foraminiferal $\delta^{18}\text{O}$ Approach. *Science* **2007**, *318*, 439–441. [[CrossRef](#)]
16. Cacho, I. Chapter 2—Quaternary Ice Ages in the Iberian Peninsula. In *Iberia, Land of Glaciers*; Oliva, M., Palacios, D., Fernández-Fernández, J.M., Eds.; Elsevier: Amsterdam, The Netherlands, 2022; pp. 13–35. ISBN 978-0-12-821941-6.

17. Bauch, H.A.; Erlenkeuser, H.; Grootes, P.M.; Jouzel, J. Implications of Stratigraphic and Paleoclimatic Records of the Last Interglaciation from the Nordic Seas. *Quat. Res.* **1996**, *46*, 260–269. [[CrossRef](#)]
18. Oppo, D.W.; Horowitz, M.; Lehman, S.J. Marine Core Evidence for Reduced Deep Water Production during Termination II Followed by a Relatively Stable Substage 5e (Eemian). *Paleoceanography* **1997**, *12*, 51–63. [[CrossRef](#)]
19. Mokeddem, Z.; McManus, J.F.; Oppo, D.W. Oceanographic Dynamics and the End of the Last Interglacial in the Subpolar North Atlantic. *Proc. Natl. Acad. Sci. USA* **2014**, *111*, 11263–11268. [[CrossRef](#)]
20. Govin, A.; Capron, E.; Tzedakis, P.C.; Verheyden, S.; Ghaleb, B.; Hillaire-Marcel, C.; St-Onge, G.; Stoner, J.S.; Bassinot, F.; Bazin, L.; et al. Sequence of Events from the Onset to the Demise of the Last Interglacial: Evaluating Strengths and Limitations of Chronologies Used in Climatic Archives. *Quat. Sci. Rev.* **2015**, *129*, 1–36. [[CrossRef](#)]
21. Deaney, E.L.; Barker, S.; van de Flierdt, T. Timing and Nature of AMOC Recovery across Termination 2 and Magnitude of Deglacial CO₂ Change. *Nat. Commun.* **2017**, *8*, 14595. [[CrossRef](#)]
22. Irvani, N.; Ninnemann, U.S.; Galaasen, E.V.; Rosenthal, Y.; Kroon, D.; Oppo, D.W.; Kleiven, H.F.; Darling, K.F.; Kissel, C. Rapid switches in subpolar North Atlantic hydrography and climate during the Last Interglacial (MIS 5e). *Paleoceanography* **2012**, *27*, PA2207. [[CrossRef](#)]
23. CLIMAP Project Members. The Last Interglacial Ocean. *Quat. Res.* **1984**, *21*, 123–224. [[CrossRef](#)]
24. Adkins, J.F.; Boyle, E.A.; Keigwin, L.; Cortijo, E. Variability of the North Atlantic Thermohaline Circulation during the Last Interglacial Period. *Nature* **1997**, *390*, 154–156. [[CrossRef](#)]
25. Hodell, D.A.; Minth, E.K.; Curtis, J.H.; McCave, I.N.; Hall, I.R.; Channell, J.E.T.; Xuan, C. Surface and Deep-Water Hydrography on Gardar Drift (Iceland Basin) during the Last Interglacial Period. *Earth Planet. Sci. Lett.* **2009**, *288*, 10–19. [[CrossRef](#)]
26. Kukla, G.J.; Bender, M.L.; de Beaulieu, J.-L.; Bond, G.; Broecker, W.S.; Cleveringa, P.; Gavin, J.E.; Herbert, T.D.; Imbrie, J.; Jouzel, J.; et al. Last Interglacial Climates. *Quat. Res.* **2002**, *58*, 2–13. [[CrossRef](#)]
27. Shackleton, N.J.; Sánchez-Goñi, M.F.; Paillet, D.; Lancelot, Y. Marine Isotope Substage 5e and the Eemian Interglacial. *Glob. Planet. Chang.* **2003**, *36*, 151–155. [[CrossRef](#)]
28. Lototskaya, A.; Ganssen, G.M. The Structure of Termination II (Penultimate Deglaciation and Eemian) in the North Atlantic. *Quat. Sci. Rev.* **1999**, *18*, 1641–1654. [[CrossRef](#)]
29. Tzedakis, P.C.; Drysdale, R.N.; Margari, V.; Skinner, L.C.; Menviel, L.; Rhodes, R.H.; Taschetto, A.S.; Hodell, D.A.; Crowhurst, S.J.; Hellstrom, J.C.; et al. Enhanced Climate Instability in the North Atlantic and Southern Europe during the Last Interglacial. *Nat. Commun.* **2018**, *9*, 4235. [[CrossRef](#)]
30. Clark, P.U.; He, F.; Golledge, N.R.; Mitrovica, J.X.; Dutton, A.; Hoffman, J.S.; Dendy, S. Oceanic Forcing of Penultimate Deglacial and Last Interglacial Sea-Level Rise. *Nature* **2020**, *577*, 660–664. [[CrossRef](#)]
31. Stoll, H.M.; Cacho, I.; Gasson, E.; Sliwinski, J.; Kost, O.; Moreno, A.; Iglesias, M.; Torner, J.; Perez-Mejias, C.; Haghypour, N.; et al. Rapid Northern Hemisphere Ice Sheet Melting during the Penultimate Deglaciation. *Nat. Commun.* **2022**, *13*, 3819. [[CrossRef](#)]
32. Brummer, G.-J.A.; Metcalfe, B.; Feldmeijer, W.; Prins, M.A.; Van 't Hoff, J.; Ganssen, G.M. Modal Shift in North Atlantic Seasonality during the Last Deglaciation. *Clim. Past* **2020**, *16*, 265–282. [[CrossRef](#)]
33. Channell, J.E.T.; Kanamatsu, T.; Sato, T.; Stein, R.; Alvarez Zarikian, C.A.; Malone, M.J. (Eds.) *Expedition 306 Scientists Expedition 306 Summary; Integrated Ocean Drilling Program: College Station, TX, USA, 2006; Volume 303/306.*
34. Wold, C.N. Cenozoic sediment accumulation on Drifts in the northern North Atlantic. *Paleoceanography* **1994**, *9*, 917–941. [[CrossRef](#)]
35. Grützner, J.; Higgins, S.M. Threshold Behavior of Millennial Scale Variability in Deep Water Hydrography Inferred from a 1.1 Ma Long Record of Sediment Provenance at the Southern Gardar Drift. *Paleoceanography* **2010**, *25*, PA4204. [[CrossRef](#)]
36. Hansen, B.; Østerhus, S. North Atlantic–Nordic Seas Exchanges. *Prog. Oceanogr.* **2000**, *45*, 109–208. [[CrossRef](#)]
37. Lozier, M.S.; Li, F.; Bacon, S.; Bahr, F.; Bower, A.S.; Cunningham, S.A.; de Jong, M.F.; de Steur, L.; deYoung, B.; Fischer, J. A Sea Change in Our View of Overturning in the Subpolar North Atlantic. *Science* **2019**, *363*, 516–521. [[CrossRef](#)]
38. Locarnini, R.A.; Mishonov, A.V.; Baranova, O.K.; Boyer, T.P.; Zweng, M.M.; Garcia, H.E.; Reagan, J.R.; Seidov, D.; Weathers, K.W.; Paver, C.R.; et al. *World Ocean Atlas 2018 Volume 1: Temperature*; NOAA Atlas NESDIS 81; U.S. Department of Commerce: Silver Spring, MD, USA, 2019; 52p.
39. Petit, T.; Mercier, H.; Thierry, V. New Insight Into the Formation and Evolution of the East Reykjanes Ridge Current and Irminger Current. *J. Geophys. Res. Oceans* **2019**, *124*, 9171–9189. [[CrossRef](#)]
40. Schlitzer, R. *Ocean Data View*; Alfred Wegner Institute: Bremerhaven, Germany, 2018.
41. Alonso-Garcia, M.; Sierro, F.J.; Kucera, M.; Flores, J.A.; Cacho, I.; Andersen, N. Ocean Circulation, Ice Sheet Growth and Interhemispheric Coupling of Millennial Climate Variability during the Mid-Pleistocene (ca 800–400 Ka). *Quat. Sci. Rev.* **2011**, *30*, 3234–3247. [[CrossRef](#)]
42. Rashid, H.; Lu, Q.Q.; Zeng, M.; Wang, Y.; Zhang, Z.W. Sea-Surface Characteristics of the Newfoundland Basin of the Northwest Atlantic Ocean during the Last 145,000 Years: A Study Based on the Sedimentological and Paleontological Proxies. *Appl. Sci.* **2021**, *11*, 3343. [[CrossRef](#)]
43. Bond, G.C.; Lotti, R. Iceberg Discharges into the North Atlantic on Millennial Time Scales during the Last Glaciation. *Science* **1995**, *267*, 1005–1010. [[CrossRef](#)]
44. Rashid, H.; Saint-Ange, F.; Barber, D.C.; Smith, M.E.; Devalia, N. Fine Scale Sediment Structure and Geochemical Signature between Eastern and Western North Atlantic during Heinrich Events 1 and 2. *Quat. Sci. Rev.* **2012**, *46*, 136–150. [[CrossRef](#)]

45. Alonso-Garcia, M.; Sierro, F.J.; Flores, J.A. Arctic Front Shifts in the Subpolar North Atlantic during the Mid-Pleistocene (800–400 Ka) and Their Implications for Ocean Circulation. *Palaeogeogr. Palaeoclimatol. Palaeoecol.* **2011**, *311*, 268–280. [[CrossRef](#)]
46. Lisiecki, L.E.; Raymo, M.E. A Pliocene-Pleistocene Stack of 57 Globally Distributed Benthic $\delta^{18}\text{O}$ Records. *Paleoceanography* **2005**, *20*, PA1003. [[CrossRef](#)]
47. Alvarez Zarikian, C.A.; Stepanova, A.Y.; Grutzner, J. Glacial–Interglacial Variability in Deep Sea Ostracod Assemblage Composition at IODP Site U1314 in the Subpolar North Atlantic. *Mar. Geol.* **2009**, *258*, 69–87. [[CrossRef](#)]
48. Obrochta, S.P.; Crowley, T.J.; Channell, J.E.T.; Hodell, D.A.; Baker, P.A.; Seki, A.; Yokoyama, Y. Climate Variability and Ice-Sheet Dynamics during the Last Three Glaciations. *Earth Planet. Sci. Lett.* **2014**, *406*, 198–212. [[CrossRef](#)]
49. Barker, S.; Chen, J.; Gong, X.; Jonkers, L.; Knorr, G.; Thornalley, D. Icebergs Not the Trigger for North Atlantic Cold Events. *Nature* **2015**, *520*, 333–336. [[CrossRef](#)]
50. De Abreu, L.; Shackleton, N.J.; Schönfeld, J.; Hall, M.; Chapman, M. Millennial-Scale Oceanic Climate Variability off the Western Iberian Margin during the Last Two Glacial Periods. *Mar. Geol.* **2003**, *196*, 1–20. [[CrossRef](#)]
51. Toucanne, S.; Zaragosi, S.; Bourillet, J.F.; Gibbard, P.L.; Eynaud, F.; Giraudeau, J.; Turon, J.L.; Cremer, M.; Cortijo, E.; Martinez, P.; et al. A 1.2Ma Record of Glaciation and Fluvial Discharge from the West European Atlantic Margin. *Quat. Sci. Rev.* **2009**, *28*, 2974–2981. [[CrossRef](#)]
52. Heinrich, H. Origin and Consequences of Cyclic Ice Rafting in the Northeast Atlantic Ocean During the Past 130,000 Years. *Quat. Res.* **1988**, *29*, 142–152. [[CrossRef](#)]
53. Grousset, F.E.; Pujol, C.; Labeyrie, L.; Auffret, G.; Boelaert, A. Were the North Atlantic Heinrich Events Triggered by the Behavior of the European Ice Sheets? *Geology* **2000**, *28*, 123. [[CrossRef](#)]
54. Channell, J.E.T.; Hodell, D.A.; Romero, O.; Hillaire-Marcel, C.; de Vernal, A.; Stoner, J.S.; Mazaud, A.; Röhl, U. A 750-Kyr Detrital-Layer Stratigraphy for the North Atlantic (IODP Sites U1302–U1303, Orphan Knoll, Labrador Sea). *Earth Planet. Sci. Lett.* **2012**, *317–318*, 218–230. [[CrossRef](#)]
55. Piper, D.J.W.; Tripsanas, E.; Mosher, D.C.; MacKillop, K. Paleoseismicity of the Continental Margin of Eastern Canada: Rare Regional Failures and Associated Turbidites in Orphan Basin. *Geosphere* **2019**, *15*, 85–107. [[CrossRef](#)]
56. Bard, E.; Rostek, F.; Turon, J.-L.; Gendreau, S. Hydrological Impact of Heinrich Events in the Subtropical Northeast Atlantic. *Science* **2000**, *289*, 1321–1324. [[CrossRef](#)] [[PubMed](#)]
57. Hodell, D.A.; Channell, J.E.T.; Curtis, J.H.; Romero, O.E.; Röhl, U. Onset of “Hudson Strait” Heinrich Events in the Eastern North Atlantic at the End of the Middle Pleistocene Transition (~640 Ka)? *Paleoceanogr. Paleoclimatol.* **2008**, *23*, PA4218. [[CrossRef](#)]
58. Margari, V.; Skinner, L.C.; Tzedakis, P.C.; Ganopolski, A.; Vautravers, M.; Shackleton, N.J. The Nature of Millennial-Scale Climate Variability during the Past Two Glacial Periods. *Nat. Geosci.* **2010**, *3*, 127–131. [[CrossRef](#)]
59. Johannessen, T.; Jansen, E.; Flatøy, A.; Ravelo, A.C. *The Relationship between Surface Water Masses, Oceanographic Fronts and Paleoclimatic Proxies in Surface Sediments of the Greenland, Iceland, Norwegian Seas*; Zahn, R., Pedersen, T.F., Kaminski, M.A., Labeyrie, L., Eds.; Springer: Berlin/Heidelberg, Germany, 1994; pp. 61–85.
60. Stangeew, E. Distribution and Isotopic Composition of Living Planktonic Foraminifera *N. pachyderma* (Sinistral) and *T. quinqueloba* in the High Latitude North Atlantic. Ph.D. Thesis, University of Kiel, Kiel, Germany, 2001.
61. Barrenechea Angeles, I.; Lejzerowicz, F.; Cordier, T.; Scheplitz, J.; Kucera, M.; Ariztegui, D.; Pawlowski, J.; Morard, R. Planktonic Foraminifera EDNA Signature Deposited on the Seafloor Remains Preserved after Burial in Marine Sediments. *Sci. Rep.* **2020**, *10*, 20351. [[CrossRef](#)]
62. Sahoo, N.; Saalim, S.M.; Matul, A.; Mohan, R.; Tikhonova, A.; Kozina, N. Planktic Foraminiferal Assemblages in Surface Sediments From the Subpolar North Atlantic Ocean. *Front. Mar. Sci.* **2022**, *8*, 781675. [[CrossRef](#)]
63. Kandiano, E.S.; Bauch, H.A.; Müller, A. Sea Surface Temperature Variability in the North Atlantic during the Last Two Glacial–Interglacial Cycles: Comparison of Faunal, Oxygen Isotopic, and Mg/Ca-Derived Records. *Palaeogeogr. Palaeoclimatol. Palaeoecol.* **2004**, *204*, 145–164. [[CrossRef](#)]
64. Chapman, M.R. Seasonal Production Patterns of Planktonic Foraminifera in the NE Atlantic Ocean: Implications for Paleotemperature and Hydrographic Reconstructions: CURRENTS. *Paleoceanography* **2010**, *25*, PA1101. [[CrossRef](#)]
65. Farmer, E.J.; Chapman, M.R.; Andrews, J.E. Holocene Temperature Evolution of the Subpolar North Atlantic Recorded in the Mg/Ca Ratios of Surface and Thermocline Dwelling Planktonic Foraminifers. *Glob. Planet. Chang.* **2011**, *79*, 234–243. [[CrossRef](#)]
66. Billups, K.; Vizcaíno, M.; Chiarello, J.; Kaiser, E.A. Reconstructing Western Boundary Current Stability in the North Atlantic Ocean for the Past 700 Kyr From *Globorotalia truncatulinoides* Coiling Ratios. *Paleoceanogr. Paleoclimatol.* **2020**, *35*, e2020PA003958. [[CrossRef](#)]
67. Bé, A.; Tolderlund, O.S. Distribution and Ecology of Living Planktonic Foraminifera in Surface Waters of the Atlantic and Indian Oceans. In *The Micropaleontology of Oceans*; Cambridge University Press: New York, NY, USA, 1971; pp. 105–149.
68. Duplessy, J.-C.; Labeyrie, L.; Juillet-leclerc, A.; Maitre, F.; Duprat, J.; Sarnthein, M. Surface Salinity Reconstruction of the North Atlantic Ocean during the Last Glacial Maximum. *Oceanol. Acta* **1991**, *14*, 311–324.
69. Elderfield, H.; Ganssen, G. Past Temperature and $\delta^{18}\text{O}$ of Surface Ocean Waters Inferred from Foraminiferal Mg/Ca Ratios. *Nature* **2000**, *405*, 442–445. [[CrossRef](#)] [[PubMed](#)]
70. Schiebel, R.; Bijma, J.; Hemleben, C. Population Dynamics of the Planktic Foraminifer *Globigerina Bulloides* from the Eastern North Atlantic. *Deep. Sea Res. Part I Oceanogr. Res. Pap.* **1997**, *44*, 1701–1713. [[CrossRef](#)]

71. Fairbanks, R.G.; Wiebe, P.H.; Bé, A.W.H. Vertical Distribution and Isotopic Composition of Living Planktonic Foraminifera in the Western North Atlantic. *Science* **1980**, *207*, 61–63. [[CrossRef](#)] [[PubMed](#)]
72. Rebotim, A.; Voelker, A.H.L.; Jonkers, L.; Waniek, J.J.; Schulz, M.; Kucera, M. Calcification Depth of Deep-Dwelling Planktonic Foraminifera from the Eastern North Atlantic Constrained by Stable Oxygen Isotope Ratios of Shells from Stratified Plankton Tows. *J. Micropalaeontol.* **2019**, *38*, 113–131. [[CrossRef](#)]
73. Mulitza, S.; Dürkoop, A.; Hale, W.; Wefer, G.; Stefan Niebler, H. Planktonic Foraminifera as Recorders of Past Surface-Water Stratification. *Geology* **1997**, *25*, 335. [[CrossRef](#)]
74. Ganssen, G.M.; Kroon, D. The Isotopic Signature of Planktonic Foraminifera from NE Atlantic Surface Sediments: Implications for the Reconstruction of Past Oceanic Conditions. *J. Geol. Soc.* **2000**, *157*, 693–699. [[CrossRef](#)]
75. Kucera, M.; Weinelt, M.; Kiefer, T.; Pflaumann, U.; Hayes, A.; Weinelt, M.; Chen, M.-T.; Mix, A.C.; Barrows, T.T.; Cortijo, E.; et al. Reconstruction of Sea-Surface Temperatures from Assemblages of Planktonic Foraminifera: Multi-Technique Approach Based on Geographically Constrained Calibration Data Sets and Its Application to Glacial Atlantic and Pacific Oceans. *Quat. Sci. Rev.* **2005**, *24*, 951–998. [[CrossRef](#)]
76. Ottens, J.J. Planktic Foraminifera as North Atlantic Water Mass Indicators. *Oceanol. Acta* **1991**, *14*, 123–140.
77. Metcalfe, B.; Feldmeijer, W.; Ganssen, G.M. Oxygen Isotope Variability of Planktonic Foraminifera Provide Clues to Past Upper Ocean Seasonal Variability. *Paleoceanogr. Paleoclimatol.* **2019**, *34*, 374–393. [[CrossRef](#)]
78. Chapman, M.R.; Shackleton, N.J. Global Ice-Volume Fluctuations, North Atlantic Ice-Rafting Events, and Deep-Ocean Circulation Changes between 130 and 70 Ka. *Geology* **1999**, *27*, 795. [[CrossRef](#)]
79. Kretschmer, M.; Coumou, D.; Agel, L.; Barlow, M.; Tziperman, E.; Cohen, J. More-Persistent Weak Stratospheric Polar Vortex States Linked to Cold Extremes. *Bull. Am. Meteorol. Soc.* **2018**, *99*, 49–60. [[CrossRef](#)]
80. Jonkers, L.; Kučera, M. Sensitivity to Species Selection Indicates the Effect of Nuisance Variables on Marine Microfossil Transfer Functions. *Clim. Past* **2019**, *15*, 881–891. [[CrossRef](#)]
81. Rodrigues, T.; Alonso-García, M.; Hodell, D.A.; Rufino, M.; Naughton, F.; Grimalt, J.O.; Voelker, A.H.L.; Abrantes, F. A 1-Ma Record of Sea Surface Temperature and Extreme Cooling Events in the North Atlantic: A Perspective from the Iberian Margin. *Quat. Sci. Rev.* **2017**, *172*, 118–130. [[CrossRef](#)]
82. Žarić, S.; Donner, B.; Fischer, G.; Mulitza, S.; Wefer, G. Sensitivity of Planktic Foraminifera to Sea Surface Temperature and Export Production as Derived from Sediment Trap Data. *Mar. Micropaleontol.* **2005**, *55*, 75–105. [[CrossRef](#)]
83. Greco, M.; Jonkers, L.; Kretschmer, K.; Bijma, J.; Kucera, M. Depth Habitat of the Planktonic Foraminifera *Neogloboquadrina pachyderma* in the northern high latitudes explained by sea-ice and chlorophyll concentrations. *Biogeosciences* **2019**, *16*, 3425–3437. [[CrossRef](#)]
84. Rufino, M.M.; Salgueiro, E.; Voelker, A.A.H.L.; Polito, P.S.; Cermeño, P.A.; Abrantes, F. Ocean Kinetic Energy and Photosynthetic Biomass Are Important Drivers of Planktonic Foraminifera Diversity in the Atlantic Ocean. *Front. Mar. Sci.* **2022**, *9*, 887346. [[CrossRef](#)]

Disclaimer/Publisher’s Note: The statements, opinions and data contained in all publications are solely those of the individual author(s) and contributor(s) and not of MDPI and/or the editor(s). MDPI and/or the editor(s) disclaim responsibility for any injury to people or property resulting from any ideas, methods, instructions or products referred to in the content.